PAPER

Check for updates

Facile hydrothermal synthesis of cobaltosic sulfide nanorods for high performance supercapacitors†

Yin Song,[a] Yuanhao Ding,[a] Chenghua Yang,[a] Xiaokang Pei,[a] Guangxia Wang,[a] Dezhou Zheng,[a] Wei Xu,[a] Fuxin Wang [ID] *[a] and Xihong Lu [ID] *[ab]

With high reactivity, electrical conductivity, theoretical specific capacitance and well redox reversibility, transition metal sulfides are considered as a promising anode material for supercapacitors. Hence, we designed a simple two-step hydrothermal process to grow Co_4S_3 nanorod arrays *in situ* on flexible carbon cloth substrates. Benefited from the larger specific surface area of nanoarrays, the binder-free Co_4S_3 electrode demonstrates a higher specific capacity of 1.97 F cm^{-2} at a current density of 2 mA cm^{-2}, while the Co_3O_4 electrode has a capacity of only 0.07 F cm^{-2} at the same current density. Surprisingly, at a high scan rate of 200 mV s^{-1}, the synthesized Co_4S_3 electrode still maintains almost 100% of its initial capacitance after 5000 cycles. Moreover, when using the prepared Co_4S_3 and MnO_2 electrode as the anode and cathode, the fabricated flexible supercapacitor obtains a high volumetric energy density of 0.87 mW h cm^{-3} (power density of 0.78 W cm^{-3}) and a peak power density of 0.89 W cm^{-3} (energy density of 0.50 mW h cm^{-3}). The excellent electrochemical properties imply that there is a large market for the prepared materials in flexible energy storage devices.

Introduction

With the continuous development of technology, especially the development of mobile electronic devices, and intelligent equipment, the demand for highly efficient energy storage equipment such as lithium-ion batteries, sodium-ion batteries, and supercapacitors has risen sharply.[1–4] Among these devices, the supercapacitors have attracted attention and study because of their high energy conversion efficiency, long cycle time (>10 000 cycles), and fast charge/discharge performance (10 s to 10 min). Compared with conventional capacitors, supercapacitors possess a relatively high energy density (1–30 W h kg^{-1}).[5–7] Based on these advantages, supercapacitors are considered to fill the gap of the batteries and conventional capacitors. Nevertheless, the energy density of supercapacitors is remain poor compared to lithium-ion batteries (about 150 W h kg^{-1}), limiting its large-scale application.[8,9] According to the equation $E = 1/2CV^2$, there are two major methods to enhance the energy storage performance of supercapacitors: (i) increasing the specific capacity of the electrode; (ii) expanding the cell voltage.[10–12] To scale up the cell voltage, the general research strategy is to replace the aqueous solution-based electrolytes with organic electrolytes or ionic liquids. However, organic electrolytes are flammable and can pose safety hazards, and the traces of water adsorbed in them still limit the further expansion of the voltage window.[13–17] Therefore, increasing the specific capacity of electrode materials becomes another key factor. The energy storage performance of supercapacitor devices can be boosted by adjusting the intrinsic properties of the electrode materials.

The electrode as a crucial component of the supercapacitors directly influences their performance. In general, electrode materials are primarily comprised of carbon materials (such as activated carbon, graphene, porous carbon), conductive polymers (such as polythiophene, polyaniline), and transition metal compounds (such as MnO_2, Co_3O_4, NiO, CoS_2 and *etc.*).[18–23] Materials based on transition metal compounds have been extensively reported because their energy densities are higher than those of electrical double-layer capacitors (carbon-based materials) and conducting polymers.[24,25] In recent years, Co-based compounds have exhibited prominent property, and have been a popular topic in the field of supercapacitors. The intrinsically high redox activity of cobalt sulfide, relative to its metal oxide analogs, and the higher electrical conductivity due to the lower optical band gap energy, are of particular interest.[26–28] Hence, a series of cobalt sulfide nanomaterials with various morphologies have been designed as electrode materials for supercapacitors, and good electrochemical properties have been obtained. For instance, Peng *et al.* synthesized CoS_2 hollow spheres with high surface area by hydrothermal method.

[a]*School of Applied Physics and Materials, Wuyi University, Jiangmen 529020, PR China. E-mail: wangfux91@126.com*

[b]*MOE of the Key Laboratory of Bioinorganic and Synthetic Chemistry, The Key Lab of Low-carbon Chem & Energy Conservation of Guangdong Province, School of Chemistry, Sun Yat-Sen University, Guangzhou 510275, PR China. E-mail: luxh6@mail.sysu.edu.cn*

† Electronic supplementary information (ESI) available. See https://doi.org/10.1039/d2ra01648f

As the anode of the supercapacitor, the CoS_2 hollow sphere electrode obtains specific capacitance of 1301 F g^{-1} at a current densities of 1 A g^{-1}.[29] Wang reported a silver fungus-like CoS obtained by mixed solvent thermal method. The electrode material exhibits a high specific capacity due to the three-dimensional pore structure. The electrode material displays a high specific capacity of 350.4 F g^{-1} at a current density of 1 A g^{-1}.[30] Moreover, a series of composite materials, such as $NiCo_2O_4$@CoS (1902.5 F g^{-1} at a current density of 1 A g^{-1}),[31] ZnO NFAs/CoS NFs (1416 F g^{-1} at a current density of 1 A g^{-1}),[32] have been designed and obtained good electrochemical properties, demonstrating the greater potential of cobalt sulfide for supercapacitor. However, there is still room for improvement in the rate performance and capacity of cobalt sulfide, and the manufacturing process is also complicated and take a long time. It is not only important but also challenging to explore facile manner so as to further improve the energy storage capacity and rate performance of cobalt sulfide materials.

In this research, Co_4S_3 nanorod arrays were prepared on flexible carbon cloth substrate by a simple two-step hydrothermal method. Benefiting from *in situ* sulfurate method, the prepared binder-free Co_4S_3 electrode possessed the high specific area, good electronic and ionic conductivity, and then obtained a significant specific capacity of 1.97 F cm^{-2} at a current density of 2 mA cm^{-2}. Additionally, the Co_4S_3 electrode also exhibited a satisfactory rate performance of 0.78 F cm^{-2} at a current density of 10 mA cm^{-2} and cycling life (almost 100% of the initial capacitance after 5000 cycles at a high scan rate of 200 mV s^{-1}). As expected, the fabricated flexible supercapacitors, composed of the as-prepared Co_4S_3 electrode and MnO_2 electrode, achieved a satisfactory volumetric energy density of 0.87 mW h cm^{-3} and power density of 0.89 W cm^{-3}.

Experimental section

Synthesis of Co_3O_4 electrode

All chemical reagents in this experiment were of analytical grade, and no further purification. Co_3O_4 nanorods arrays were prepared by hydrothermal method using flexible conductive carbon cloth as the substrate. Firstly, the carbon cloth was cut into pieces, each 2 cm × 3 cm large, and then sonicated in deionized water, ethanol solution and acetone solution for 10 min, respectively. 10 mmol of $Co(NO_3)_2 \cdot 6H_2O$ was dissolved in 40 mL of ethanol solution, with the cleaned carbon cloth immersed in the solution for 10 min, and then heated on a heating plate at 400 °C for 10 min, and repeated four times. Then, 5 mmol of $Co(NO_3)_2 \cdot 6H_2O$, 10 mmol of NH_4F and 25 mmol of CH_4N_2O were added to a beaker with 50 mL of deionized water, and stirred to entirely dissolution. The prepared solution was moved to a 25 mL Teflon-lined autoclave with the pretreated carbon cloth. Lastly, the Teflon-lined autoclave was placed in an oven and kept at 120 °C for 5 h. After natural cooling, the pink Co_3O_4 powder was evenly grown on the surface of carbon fiber, before it was washed with deionized water.

Synthesis of Co_4S_3 electrode

The above prepared Co_3O_4 material was put in an autoclave with Teflon-lined together with 0.3 M Na_2S solution. Then it was placed in an oven at 80, 120, 150, and 180 °C for 6 h. After naturally cooling to room temperature, Co_4S_3-X (X is the 80, 120, 150, 180 °C) electrodes were obtained.

Synthesis of MnO_2 electrode

MnO_2 electrodes were prepared based on the previous literature.[33] In brief, MnO_2 nanomaterial was electrodeposited on a flexible carbon cloth substrate through a CHI660E electrochemical work-station with a three-electrode system, which was composed of clean carbon cloth as working electrode, carbon rod as auxiliary electrode, and saturated calomel electrode as reference electrode. The electrodeposition solution was a mixture of 0.1 mol L^{-1} $(CH_3COO)_2Mn$ and 0.1 mol L^{-1} Na_2SO_4. The experiment to make the MnO_2 electrode was performed at 1.0 V for 30, 60, 90, 120, and 240 s, respectively.

Fabrication of asymmetric supercapacitors (ASCs)

The solid-state ASCs were made up of a NKK separator, PVA/LiCl gel, and the prepared MnO_2 and Co_4S_3 electrodes. Firstly, LiCl (11.48 g), PVA (6 g), and DI water (50 mL) were mixed with magnetic stirring at 80 °C for 30 min. Then the prepared electrodes and separator were dipped in the above solution. After packing, the prepared ASCs was kept at 40 °C for 12 h to eliminate extra water from the electrolyte.

Materials characterization

The morphology, crystal type, and microstructure of the prepared materials were characterized by X-ray diffraction (XRD, X'Pert Pro MPD, PANalytical) with Cu K$_\alpha$ radiation, transmission electron microscopy (TEM, JEM-F200, JEOL), and field-emission scanning electron microscopy (SEM, Sigma500, ZEISS). X-ray photoelectron spectroscopy (XPS, NEXSA, Thermo VG) and Raman Spectroscopy (LabRAM HR Evolution, HORIBA) were used to research the element composition and functional group distribution of the synthesized materials. Cyclic voltammetry (CV), galvanostatic charge–discharge (GCD) curves, electrochemical impedance spectra (EIS) of the electrodes were performed on an electrochemical workstation with a three-electrode system, while the prepared electrodes, carbon rod electrode, SCE electrode served as the work electrode, counter electrode, and reference electrode, respectively. The electrochemical performance of the prepared asymmetric supercapacitors was also tested by an electrochemical workstation (CHI660E).

Results and discussion

The Co_3O_4 electrodes were manufactured by a simple hydrothermal method. Briefly, the Co_3O_4 nanomaterials were synthesized hydrothermally with the use of $Co(NO_3)_2 \cdot 6H_2O$, NH_4F, and CH_4N_2O on a flexible carbon cloth substrate (details can be seen in the Experimental section). As seen in Fig. 1a and
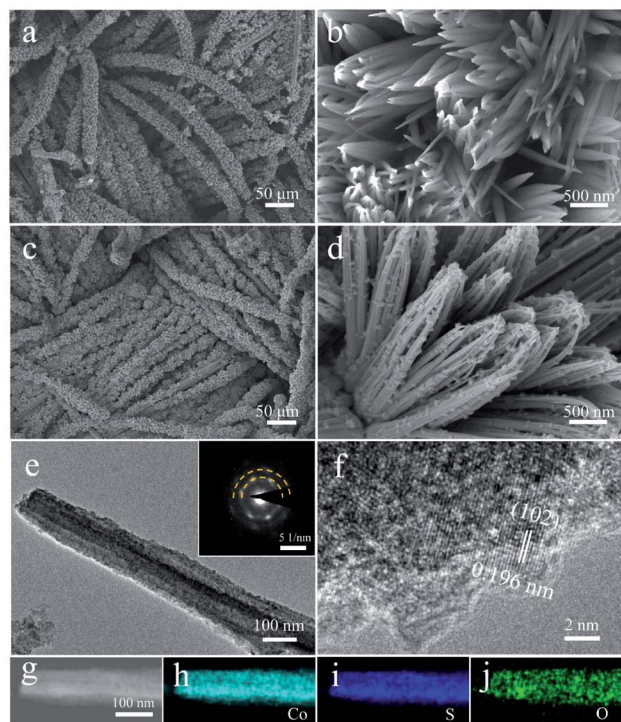
Fig. 1 (a, b) SEM image of the Co_3O_4 sample. (c, d) SEM images of the Co_4S_3 sample. (e) TEM image of the Co_4S_3 sample (insert the corresponding SAED pattern). (f) HRTEM of the Co_4S_3 sample. (g–j) The corresponding area mapping results of Co_4S_3 sample.

b, the Co_3O_4 nanorods were evenly coated on the carbon fiber. Then, they were vulcanized to Co_4S_3 by Na_2S through secondary hydrothermal treatment. Fig. 1c and d show that the nanorod arrays remained coated on the surface of the carbon fiber. However, the surface of the Co_4S_3 nanorods is rougher compared to that of the Co_3O_4. As shown in Fig. S1,† Co_4S_3 obtained a larger specific surface area (9.6 m² g⁻¹) than Co_3O_4 (6.8 m² g⁻¹), indicating that it has more active sites. The length of the nanorods was about 4 μm and the average diameter reached 0.2 μm. To further study the microstructure of the electrode materials, a TEM study was performed. Fig. 1e and S2† show that both Co_3O_4 and Co_4S_3 electrodes possess the nanorods, corresponding to the SEM results. Selected area electron diffraction (SAED) pattern proves the well crystallinity of Co_4S_3 nanomaterial (inset in Fig. 1e). Two clear diffraction rings well correspond to the hexagonal crystal system of Co_4S_3 (101), (110) crystal planes (JCPDF#02-1458). From the high resolution transmission electron microscopy (HRTEM) in Fig. 1f, it can be seen that the nanorods are crystalline with a crystal plane spacing of 0.196 nm, corresponding to the (102) plane of Co_4S_3 (JCPDS#02-1458), which is consistent with the SAED results. Then, EDS energy spectrum analysis was performed on the nanorods. From Fig. 1g–j, it can be seen that the Co, S, and O elements are uniformly distributed on the nanorods.

To further characterize the crystal types, XRD, Raman, and XPS were utilized to study the functional group, and valence composition of the synthesized materials. As shown in Fig. 2a, the characteristic diffraction peaks of the synthesized materials
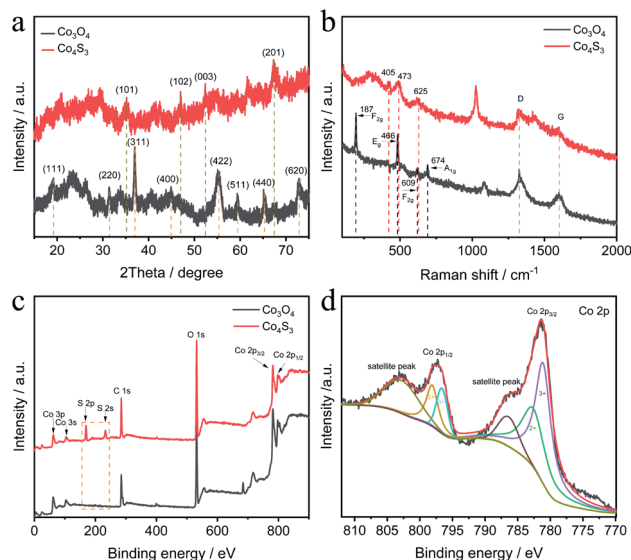
are in good accordance with the Co_3O_4 (JCPDS#42-1467) and Co_4S_3 (JCPDS#02-1458), respectively. The comparison of the characteristic peaks indicates that the Co_3O_4 has been completely converted to Co_4S_3 by the secondary hydrothermal of sulfidation reaction. The Raman spectra of Co_3O_4 and Co_4S_3
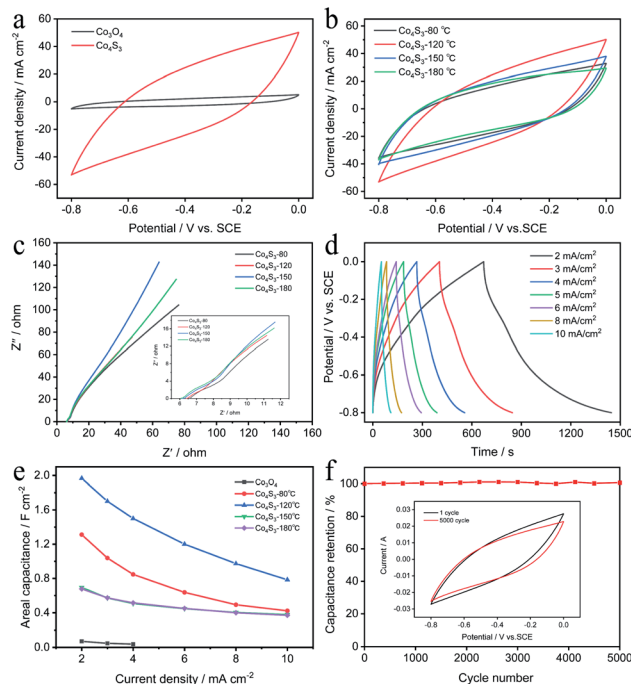

Fig. 2 (a) XRD spectra of the Co_3O_4 and Co_4S_3 sample. (b) Raman spectra of the Co_3O_4 and Co_4S_3 sample. (c) The XPS survey spectra of the Co_3O_4 and Co_4S_3 sample. (d) Co 2p spectra of the Co_4S_3 sample.

Fig. 3 (a) CV curves of the Co_3O_4 and Co_4S_3 electrodes at a scan of 100 mV s⁻¹. (b) CV curves of the Co_4S_3 electrodes at different temperature. (c) EIS of the Co_4S_3 electrode at different temperature. (d) GCD curves of Co_4S_3-120 electrode at different current density. (e) Rate performance of the different electrode. (f) Cycle performance of the Co_4S_3-120 electrode.

are presented in Fig. 2b. It can be clearly seen that there are four characteristic peaks at 187, 466, 512, 609, and 674 cm^{-1} in the Co_3O_4 sample, which correspond to the molecular vibration of F_{2g}, E_g, F_{2g}, F_{2g}, and A_{1g}, respectively.[33,34] Meanwhile, the peak at 473, 517, 683 cm^{-1} are attributed to the E_g, F_{2g}, A_{1g} modes of cobalt sulfide,[35] which further confirm that the complete sulfidation of Co_3O_4 to Co_4S_3. It is worth noting that both samples show two characteristic peaks at about 1350 and 1580 cm^{-1}, originating from carbon cloth substrate, representing the D band and G band of carbon, respectively.[36] To further investigate the surface compositions of Co_4S_3, XPS tests were performed and the results shown in Fig. 2c. In the survey spectrum, both Co_4S_3 and Co_3O_4 samples contain the Co and O elements, and only Co_4S_3 contains sulfur element, which is in line with the EDS results. As indicated in Fig. 2d, there are four peaks of satellite peak, Co $2p_{1/2}$ peak, satellite peak, and Co $2p_{1/2}$ peak evident in the graph. Further analysis the core level of Co 2p peaks shows that the two peaks located at 780.7 eV and 796.5 eV attributed to the $2p_{3/2}$ and $2p_{1/2}$ of Co^{2+}, while the peaks at 778.4 eV and 793.3 eV are originate from the Co^{3+} $2p_{3/2}$ and Co^{3+} $2p_{1/2}$.[33,37] The core level spectrum of Co 2p XPS results further prove that Co_4S_3 have been completely synthesized. The core level S 2p spectrum (Fig. S3a†) shows two peaks with binding energy values of 162.0 eV and 169.0 eV, consistent with the S 2p and oxidized sulfur. In addition, as shown in Fig. S3b,† the fitting peaks at 161.6 eV and 163.0 eV can be ascribed to the $2p_{3/2}$ and $2p_{1/2}$ of sulfur in Co_4S_3.[37,38]

To investigate the electrochemical performance of the Co_4S_3 electrode, a three-electrode system was constructed with 5 M LiCl as the electrolyte, Co_4S_3 electrode as the working electrode, SCE as the reference electrode, and carbon rod as the counter electrode with a potential window between −0.8 and 0 V. Firstly, the cyclic voltammetry (CV) curves of the synthesized Co_3O_4 and Co_4S_3 electrodes were collected at a scan of 100 mV s^{-1} in Fig. 3a. It is clear that the electrochemical properties of the materials have been greatly improved by sulphuration treatment, while the specific capacitance was proportional to the average area of a CV curve. Then the sulphuration temperature was optimized (Fig. 3b). It could be clearly seen that the Co_4S_3 electrode obtained at 120 °C displays the largest area of the CV curves than that of the other reaction temperatures (80, 150, and 180 °C). Fig. 3c shows the electrochemical impedance spectra (EIS) of Co_4S_3 electrodes at different reaction temperature, where R_s and R_{ct} represented the internal resistance, and charge transfer resistance respectively. They mainly consist of semicircle in high frequency region and lines in the low frequency region. The semicircles are mainly caused by the chemical reaction between the electrode material and the electrolyte, and the lines represent the ion diffusion resistor. The charge-transfer resistance for the Co_4S_3 electrode is only 0.9 Ω, which is smaller compared with that for other electrodes at different temperatures, demonstrating the superiority of the Co_4S_3 electrode in conductivity. Fig. 3d and S4† show the GCD and CV curves of Co_4S_3 electrode at 120 °C at different current densities and scan rates. And the specific capacity of Co_4S_3 and the different reaction temperature are calculated based on GCD curves of the fabricated electrodes. As shown in Fig. 3e, the specific capacity of Co_4S_3 is 1.97 F cm^{-2}

at 2 mA cm^{-2} and 0.78 F cm^{-2} at 10 mA cm^{-2}, which indicates its excellent rate capacity (a 5-fold increase in the scan rate and the Co_4S_3 electrode still maintains 39.6% of its initial capacitance). Fig. 3f shows the cycling performance of the Co_4S_3 electrode at a high scan rate of 200 mV s^{-1}. After 5000 cycles, 96.6% of the specific capacity is retained, which shows that the synthesized electrode is rather stable. The inset in Fig. 3f shows the CV curves before and after 5000 cycles.

The assembly of asymmetric supercapacitor devices is a proven method in increasing the energy density of supercapacitors, allowing for a wide range of operating potentials using different positive and negative electrodes. Hence, a simple ASCs device was assembled from a MnO_2 electrode (electroplating for 120 s) as the cathode and a Co_4S_3 electrode as the anode (denoted as MnO_2//Co_4S_3-ASCs) (see Experimental section for details). For the best capacity of the ASCs device, the balance of the charges of the cathode and anode materials should be achieved before assembly. As shown in Fig. 4a, the CV curves of the cathode and anode were first compared, and it can be seen that the area ratio of about 5 : 6. Fig. 4b shows the CV curves of the assembled ASCs devices gathered at different potential windows. As a result, the potential window of MnO_2//Co_4S_3-ASCs can be stably extended to 1.8 V, indicating that the device has a good energy storage capacity. All these CV curves at different scan rates exhibit regular rectangle, even at high scan rate of 100 mV s^{-1} (Fig. S5†). In addition, the GCD curves of MnO_2//Co_4S_3-ASCs at different current densities were also collected

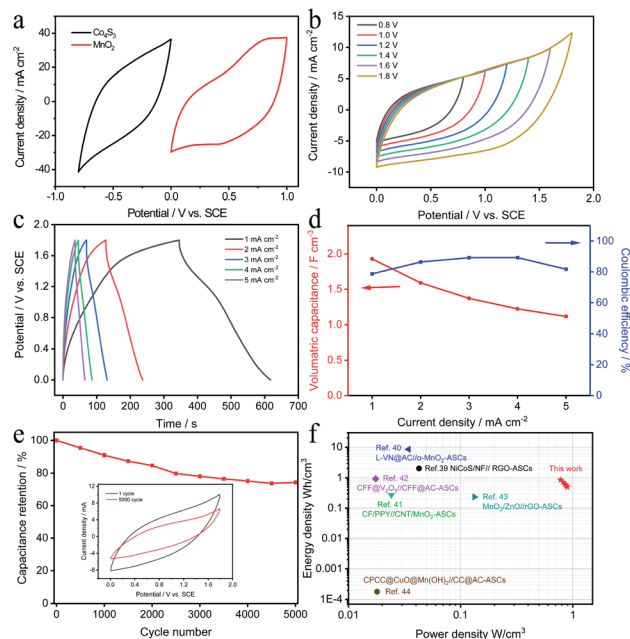**Fig. 4** (a) CV curves of MnO_2 and Co_4S_3 electrodes at a scan rate of 100 mV s^{-1}. (b) CV curves of the as-assembled MnO_2//Co_4S_3-ASCs device collected with different potential windows. (c) GCD curves of MnO_2//Co_4S_3-ASCs collected at various current densities. (d) Volumetric capacitance of MnO_2//Co_4S_3-ASCs calculated from GCD curves as a function of current density. (e) Cycling performance of MnO_2//Co_4S_3-ASCs at a scan of 100 mV s^{-1}. (f) Ragone plots of the as-assembled MnO_2//Co_4S_3-ASCs.

(Fig. 4c). It can be clearly seen that these GCD curves show good symmetry, indicating that MnO_2//Co_4S_3-ASCs has a satisfactory capacitive behavior and fast charge/discharge characteristics. The volumetric specific capacitance of the assembled MnO_2//Co_4S_3-ASCs can be measured by calculating the discharge time of the GCD curves. As displayed in Fig. 4d, MnO_2//Co_4S_3-ASCs obtained a high volumetric capacitance of 1.9 F cm^{-3} at a current of 1 mA cm^{-2}. As the current density increases, its specific capacitance gradually decreases. While the current density raised to 5 mA cm^{-2}, it still has a specific capacity of 1.1 F cm^{-3}, which is 57.9% of that at the current of 1 mA cm^{-2}. This result indicates that the assembled devices have a good rate capacity. In addition, all the coulombic efficiencies remain above 84%, indicating its prominent capacitive behavior. The cycling stability of the assembled MnO_2//Co_4S_3-ASCs was conducted at a scan rate of 100 mV s^{-1}. Fig. 4e shows the cycling performance of the device, and it can be seen that the capacity retention is 80% after 5000 cycles, indicating that the device possesses a relatively good cycling stability. In addition, energy density and power density are two critical factors to assess the property of device. Therefore, calculations based on the GCD curves can be performed to obtain a maximum volumetric energy density of 0.87 mW h cm^{-3} and a power density of 0.89 W cm^{-3} (Fig. 4f), which is superior to other recently reported devices, such as NiCoS/NF//r-GO-based ASCs (2.04 mW h cm^{-3} and 42.64 mW cm^{-3}),[39] L-VN@AC//α-MnO_2-based ASCs (8.5 mW h cm^{-3} and 34.3 mW cm^{-3}),[40] CF/PPY//CNT/MnO_2-based ASCs (0.27 mW h cm^{-3} and 24.1 mW cm^{-3}),[41] CFF@V_2O_5//CFF@AC-based ASCs (0.928 mW h cm^{-3} and 17.5 mW cm^{-3}),[42] MnO_2/ZnO//rGO-based ASCs (0.234 mW h cm^{-3} and 133 mW cm^{-3}),[43] CPCC@CuO@Mn(OH)$_2$//CC@AC-based ASCs (0.18 mW h cm^{-3} and 18 mW cm^{-3}).[44] All the results prove the high performance and practicality of the synthesized electrodes.

Conclusions

In conclusion, the Co_4S_3 nanorod arrays were successfully grown on flexible carbon cloth substrate by a two-step hydrothermal method. Benefiting from the larger specific surface area of the nanoarray, the binder-free Co_4S_3 electrode obtained more active sites with a high specific capacity of 1.97 F cm^{-2} at a current density of 2 mA cm^{-2}, which is much higher than that of the Co_3O_4 electrode (0.07 F cm^{-2}). Satisfactorily, the Co_4S_3 electrode exhibited a long cycling stability, with its initial capacitance remaining almost at 100% after 5000 cycles at a high scan rate of 200 mV s^{-1}. Moreover, the assembled flexible MnO_2//Co_4S_3-ASCs obtained a maximum volumetric energy density of 0.87 mW h cm^{-3} and power density of 0.89 W cm^{-3}.

Conflicts of interest

There are no conflicts to declare.

Acknowledgements

References

1 Y. Zhou, H. Qi, J. Yang, Z. Bo, F. Huang, M. S. Islam, X. Lu, L. Dai, R. Amal and C. H. Wang, *Energy Environ. Sci.*, 2021, **14**, 1854–1896.

2 Y. Zheng, Y. Yao, J. Ou, M. Li, D. Luo, H. Z. Dou, Z. Q. Li, K. Amine, A. P. Yu and Z. Chen, *Chem. Soc. Rev.*, 2020, **49**, 8790–8839.

3 Y. Wan, K. Song, W. Chen, C. Qin, X. Zhang, J. Zhang, H. Dai, Z. Hu, P. Yan, C. Liu, S. Sun, S. Chou and C. Shen, *Angew. Chem., Int. Ed.*, 2021, **60**, 11481–11486.

4 W. Cheng, J. Fu, H. Hu and D. Ho, *Adv. Sci.*, 2021, **8**, 2100775.

5 J. Zhao and A. F. Burke, *J. Energy Chem.*, 2021, **59**, 276–291.

6 M. Mansuer, L. Miao, D. Zhu, H. Duan, Y. Lv, L. Li, M. Liu and L. Gan, *Mater. Chem. Front.*, 2021, **5**, 3061–3072.

7 P. Xie, W. Yuan, X. Liu, Y. Peng, Y. Yin, Y. Li and Z. Wu, *Energy Storage Mater.*, 2021, **36**, 56–76.

8 S. Zhao, K. Yan, J. Zhang, B. Sun and G. Wang, *Angew. Chem., Int. Ed.*, 2021, **60**, 2208–2220.

9 Z. Li, J. Lin, B. Li, C. Yu, H. Wang and Q. Li, *J. Energy Storage*, 2021, **44**, 103437.

10 J. Qin, S. Wang, F. Zhou, P. Das, S. Zheng, C. Sun, X. Bao and Z. Wu, *Energy Storage Mater.*, 2019, **18**, 397–404.

11 Y. Shao, M. F. El-Kady, J. Sun, Y. Li, Q. Zhang, M. Zhu, H. Wang, B. Dunn and R. B. Kaner, *Chem. Rev.*, 2018, **118**, 9233–9280.

12 Z. She, D. Ghosh and M. A. Pope, *ACS Nano*, 2017, **11**, 10077–10087.

13 M. Yu, D. Lin, H. Feng, Y. Zeng, Y. Tong and X. Lu, *Angew. Chem., Int. Ed.*, 2017, **56**, 5454–5459.

14 W. Zuo, C. Xie, P. Xu, Y. Li and J. Liu, *Adv. Mater.*, 2017, **29**, 1703463.

15 L. Liu, J. Niu, Z. Zhang and F. Wang, *ACS Appl. Energy Mater.*, 2021, **4**, 7751–7758.

16 L. Han, H. Huang, X. Fu, J. Li, Z. Yang, X. Liu, L. Pan and M. Xu, *Chem. Eng. J.*, 2020, **392**, 123733.

17 X. Li, Y. Tao, J. Song, W. Yang, M. Wang, C. Zhu, W. Zhao, J. Zheng and Y. Lin, *Carbon*, 2018, **129**, 236–244.

18 S. Y. Lu, M. Jin, Y. Zhang, Y. B. Niu, J. C. Gao and C. M. Li, *Adv. Energy Mater.*, 2018, **8**, 1702545.

19 X. Gang, M. Krishnamoorthy, W. Jiang, J. Pan and X. Liu, *Carbon*, 2021, **171**, 62–71.

20 M. Y. Zhang, Y. Song, D. Yang, Z. Qin, D. Guo, L. J. Bian, X. G. Sang, X. Sun and X. X. Liu, *Adv. Funct. Mater.*, 2021, **31**, 2006203.

21 X. Jin, L. Song, H. Yang, C. Dai, Y. Xiao, X. Zhang, Y. Han, C. Bai, B. Lu, Q. Liu, Y. Zhao, J. Zhang, Z. Zhang and L. Qu, *Energy Environ. Sci.*, 2021, **14**, 3075–3085.

22 C. Tang, K. Zhao, Y. Tang, F. Li and Q. Meng, *Electrochim. Acta*, 2021, **375**, 137960.

23 R. Ahmed and G. Nabi, *J. Energy Storage*, 2021, **33**, 102115.

24 R. Liu, A. Zhou, X. Zhang, J. Mu, H. Che, Y. Wang, T. Wang, Z. Zhang and Z. Kou, *Chem. Eng. J.*, 2021, **412**, 128611.

25 H. Yang, H. Guo, K. Pang, P. Fan, X. Li, W. Ren and R. Song, *Nanoscale*, 2020, **12**, 7024–7034.

26 Y. Zhao, Z. Shi, T. Lin, L. Suo, C. Wang, J. Luo, Z. Ruan, C. A. Wang and J. Li, *J. Power Sources*, 2019, **412**, 321–330.

27 M. Wang, J. Yang, S. Liu, C. Hu and J. Qiu, *ACS Appl. Energy Mater.*, 2020, **3**, 6977–6984.

28 L. Lin, Y. Ding, H. Huang, D. Yu, S. Zhang, H. Chen, S. Ramarkrishna and S. Peng, *J. Colloid Interface Sci.*, 2019, **540**, 389–397.

29 S. Peng, L. Li, H. Tan, R. Cai, W. Shi, C. Li, S. G. Mhaisalkar, M. Srinivasan, S. Ramakrishna and Q. Yan, *Adv. Funct. Mater.*, 2014, **24**, 2155–2162.

30 H. Wang, *J. Energy Storage*, 2021, **40**, 102764.

31 W. D. Wang, X. F. Li, P. P. Zhang, B. Q. Wang, S. H. Gong, X. C. Wang, F. Liu and J. P. Cheng, *J. Electroanal. Chem.*, 2021, **891**, 115257.

32 H. Chen, S. Xiao, Y. Li, X. Ma, Y. Huang, Y. Wang, J. S. Chen and Z. Feng, *Chem. Commun.*, 2021, **57**, 10520–10523.

33 W. Xu, J. Chen, M. Yu, Y. Zeng, Y. Long, X. Lu and Y. Tong, *J. Mater. Chem. A*, 2016, **4**, 10779–10785.

34 S. Yang, Y. Liu, Y. Hao, X. Yang, W. Goddard, X. Zhang and B. Cao, *Adv. Sci.*, 2018, **5**, 1700659.

35 M. Shi, Q. Wang, J. Hao, H. Min, H. You, X. Liu and H. Yang, *Dalton Trans.*, 2020, **49**, 14115–14122.

36 Q. Li, Y. Jiang, Z. Jiang, J. Zhu, X. Gan, F. Qin, T. Tang, W. Luo, N. Guo, Z. Liu, L. Wang, S. Zhang, D. Jia and Z. Fan, *Carbon*, 2022, **191**, 19–27.

37 G. Liu, B. Wang, L. Wang, T. Liu, T. Gao and D. Wang, *RSC Adv.*, 2016, **6**, 54076–54086.

38 Z. Gao, C. Chen, J. Chang, L. Chen, P. Wang, D. Wu, F. Xu and K. Jiang, *Chem. Eng. J.*, 2018, **343**, 572–582.

39 P. Prabakaran, S. Prabhu, M. Selvaraj, M. Navaneethan, P. Ramu and R. Ramesh, *J. Mater. Sci.: Mater. Electron.*, 2021, **21**, 07251.

40 G. Qu, Z. Wang, X. Zhang, S. Zhao, C. Wang, G. Zhao, P. Hou and X. Xu, *Chem. Eng. J.*, 2022, **429**, 132406.

41 Y. Xu, Y. Yan, W. Lu, S. Yarlagadda and G. Xu, *ACS Appl. Energy Mater.*, 2021, **4**, 10639–10645.

42 M. You, W. Zhang, X. Yan, H. Jiang, J. Miao, Y. Li, W. Zhou, Y. Zhu and X. Cheng, *Ceram. Int.*, 2021, **47**, 3337–3345.

43 Z. Wang, Z. Zhu, J. Qiu and S. Yang, *J. Mater. Chem. C*, 2014, **2**, 1331–1336.

44 Y. Wang, Y. Zhang, D. Dubbink and J. E. Elshof, *Nano Energy*, 2018, **49**, 481–488.